NEOPLASIA
www.neoplasia.com

Volume 15 Number 3 March 2013 pp. 335–347 335

# Anti–HER3 Domain 1 and 3 Antibodies Reduce Tumor Growth by Hindering HER2/HER3 Dimerization and AKT-Induced MDM2, XIAP, and FoxO1 Phosphorylation[1,2]

**Yassamine Lazrek[*,†], Olivier Dubreuil[†], Véronique Garambois[*], Nadège Gaborit[*], Christel Larbouret[*], Christophe Le Clorennec[*], Gaelle Thomas[*], Wilhem Leconet[*], Marta Jarlier[‡], Martine Pugnière[*], Nadia Vié[*], Bruno Robert[*], Céline Monnet[†], Khalil Bouayadi[†], Hakim Kharrat[†], Philippe Mondon[†], André Pèlegrin[*] and Thierry Chardès[*]**

[*]Institut de Recherche en Cancérologie de Montpellier, INSERM Unit 896, Université Montpellier 1, CRLC Val d'Aurelle Paul Lamarque, Montpellier, France; [†]Millegen SA, Labège, France; [‡]Unité de Biostatistiques, CRLC Val d'Aurelle Paul Lamarque, Montpellier, France

## Abstract

Blockade of the human epidermal growth factor receptor 3 (HER3) and of the downstream phosphatidylinositide 3-kinase (PI3K)/AKT pathway is a prerequisite for overcoming drug resistance and to develop novel treatments for cancers that are not eligible for the currently approved targeted therapies. To this end, we generated specific antibodies (Abs) against domain 1 (D1) and domain 3 (D3) of HER3 that recognize epitopes that do not overlap with the neuregulin-binding site. The fully human H4B-121 Ab and the mouse monoclonal Abs 16D3-C1 and 9F7-F11 inhibited tumor growth in nude mice xenografted with epidermoid, pancreatic, or triple-negative breast cancer cells. The combination of one anti-HER3 Ab and trastuzumab improved tumor growth inhibition in mice xenografted with $HER2^{low}$ cancer cell lines, for which trastuzumab alone shows no or moderate efficiency. Ab-induced disruption of tumor growth was associated with $G_1$ cell cycle arrest, proliferation inhibition, and apoptosis of cancer cells. Anti-HER3 Abs blocked HER2/HER3 heterodimerization and HER3 phosphorylation at the cell membrane, leading to inhibition of phosphorylation of the downstream AKT targets murine double minute 2, X-linked inhibitor of apoptosis, and forkhead box O1. This study demonstrates that anti–HER3 D1 and D3 Abs could represent a new option for immunotherapy of pancreatic and triple-negative breast cancers.

*Neoplasia (2013) 15, 335–347*

## Introduction

Cell plasticity is one of the main cancer features and leads to the rapid therapeutic escape of tumor cells following the initial response. The human epidermal growth factor receptor (HER) family includes four distinct receptors [epidermal growth factor receptor (EGFR; HER1 or ErbB1), HER2, HER3, and HER4] and 11 ligands [e.g., EGF and neuregulins (NRGs)] and is one of the most extensively studied plasticity network [1]. The HER3 receptor retains low level of kinase activity, sufficient to trans-autophosphorylate its intracellular region [2]. After binding to NRG, HER3 is mainly activated through heterodimerization with other tyrosine kinase receptors, and the level of expression and composition of such heterodimers play a role in the diversification of downstream signaling and oncogenic effects. Such

Abbreviations: Ab, antibody; NRG, neuregulin; PBS, phosphate-buffered saline; TR-FRET, time-resolved fluorescence resonance energy transfer; XIAP, X-linked inhibitor of apoptosis; FoxO1, forkhead box O1; MDM2, murine double minute 2; GSK3, glycogen synthase kinase 3

Address all correspondence to: Thierry Chardès, PhD, Institut de Recherche en Cancérologie de Montpellier, INSERM Unit 896, Université Montpellier 1, CRLC Val d'Aurelle Paul Lamarque, 208 rue des Apothicaires, 34298 Montpellier Cedex 5, France. E-mail: thierry.chardes@inserm.fr

[1]This work was supported by grants from the Ligue Nationale Contre le Cancer, Comité de l'Hérault, from the AAP13 Fonds Unique Interministériel, and from the LabEx MabImprove. Y.L. is supported by a Convention Industrielle de Formation par la Recherche doctoral studentship from the Agence Nationale de la Recherche et de la Technologie. Y.L., O.D., K.B., H.K., and P.M. are employed by Millegen SA.

[2]This article refers to Supplementary Materials and are available online at www.neoplasia.com.

Received 23 November 2012; Revised 16 January 2013; Accepted 18 January 2013


DOI 10.1593/neo.121960

plasticity depends on the level of stimulation, nature of the ligand, cell type, and receptor density and can be affected by exposure to antibodies (Abs) [3] that might thus contribute to HER3 regulation [4]. A specific feature of HER3 signaling activity is its unique ability to directly activate the PI3K/AKT axis, which is at the crossroad of many downstream pathways that involve the apoptosis-related proteins murine double minute 2 (MDM2), forkhead box O1 (FoxO1), and X-linked inhibitor of apoptosis (XIAP), the proliferation-related proteins cyclin-dependent kinase inhibitor 1B and glycogen synthase kinase 3 (GSK3), and the ribosomal protein S6 [5]. Consequently, the PI3K/AKT pathway controls different biologic processes, such as cell growth, survival and apoptosis, nutrient sensing, and metabolic regulation and is implicated in tumor initiation and progression. Indeed, *HER3* genetic ablation impairs *in vivo* PI3K/AKT-dependent mammary tumorigenesis [6].

HER3 expression correlates with tumor progression and reduced survival of patients with pancreatic [7], breast [8], and ovarian cancers [9], malignant melanoma and metastases [10], gastric carcinoma [11], and head and neck squamous cell carcinoma [12]. HER3 overexpression is significantly associated with poor prognosis [13] and worse metastasis-free survival [14] in colorectal carcinomas. Importantly, in breast cancer, patients with *HER2* non-amplified tumors are not eligible for trastuzumab treatment and often these tumors are "programmed" to express HER3 [8]. Similarly, pancreatic cancers, which are not eligible for targeted therapies, also show programmed HER3 overexpression [7]. Moreover, *HER2*-amplified breast tumors, which become resistant to trastuzumab after prolonged treatment, are "reprogrammed" to strongly express HER3 [15] Cetuximab resistance is also associated with HER3 overexpression in lung [16], colorectal [17], and pancreatic [18] cancers, together with deregulation of EGFR internalization/degradation [16,18]. Overexpression of HER3 and activation of the PI3K/AKT pathway are also implicated in the development of resistance to treatment with tyrosine kinase [19,20] and PI3K [21] inhibitors, insulin-like growth factor 1 receptor (IGF1R)-specific Abs [22], chemotherapeutic agents, and endocrine therapies.

Therefore, HER3 could be involved in the efficacy reduction of many approved cancer monotherapies over time by 1) leading to oversensitivity to HER3 ligands, such as NRGs [17], 2) switching heterodimerization partner within the HER family or with other kinase receptors [16,19], and 3) compensatory up-regulation of signaling pathways [23]. Indeed, the current view is that EGFR-, HER2-, or PI3K/AKT-targeted therapies (and probably other kinase receptor–triggered pathways) will not be effective in the long term unless combined with HER3 antagonists [21]. Most HER3-specific Abs described to date act by blocking the NRG-binding site [13,24–29]. However, as HER3 plays a key role in both ligand-independent and ligand-dependent oncogenic signaling [5] through paracrine or autocrine loops [30], we postulated that anti-HER3 Abs that are not restricted to the ligand-binding site might have a wider scope of action and could be associated with Abs that target the NRG-binding site for a wider spectrum of action. The therapeutic efficacy of the anti-EGFR Ab matuzumab [31], which does not target the EGF-binding site, indicates that Abs that are not directed against ligand-binding sites can have very interesting therapeutic perspectives in oncology. We thus generated Abs that bind to motifs located on domain 1 (D1), domain 3 (D3), and domain 4 (D4) of HER3 and that, for some of them, do not overlap with the NRG-binding site. These Abs reduced tumor growth in mice xenografted with different cancer cell lines, independently of their NRG addiction or triple-negative status. These Abs reduced HER2/HER3 heterodimerization at the cell membrane of tumor cells and inhibited AKT-induced phosphorylation of MDM2, FoxO1, XIAP, S6, and GSK3, leading to reduced survival of tumor cells.

## Materials and Methods

### *Reagents*

Trastuzumab was obtained from Roche Pharma AG (Grenzach-Wyhlen, Germany). The anti-HER2 Ab FRP5 was kindly provided by Nancy Hynes (Basel, Switzerland). For Western blot analysis, anti-HER2, anti-HER3, anti–phospho-HER3 (Tyr1289), anti-AKT, anti–phospho-Ser$^{473}$ and anti–Thr$^{308}$ AKT, anti–phospho-MDM2, anti-FoxO1, anti-S6, and anti–GSK3 α/β Abs were purchased from Cell Signaling Technology (Beverly, MA). The anti–glyceraldehyde 3-phosphate dehydrogenase (GAPDH) Ab was purchased from Millipore (Billerica, MA). The anti–phospho-HER2 (Tyr$^{1196}$) and anti–HER3 (Tyr$^{1262}$) Abs, mouse and human HER3 (extracellular)–Fc recombinant proteins, the Fc recombinant fragment, and the human recombinant NRG extracellular domain (ECD) were from RD Systems (Minneapolis, MN). The anti–phospho-XIAP and anti–cyclin-dependent kinase inhibitor 1B Abs were from Abcam (Cambridge, United Kingdom) and Epitomics (Burlingame, CA), respectively. The irrelevant Px Ab, used for control experiments, is an $IgG_1$ monoclonal Ab that was purified from the mouse myeloma cell line P3X63Ag8. Recombinant human HER3 was acquired from Sino Biologicals (Beijing, China).

### *Cell Lines*

The human pancreatic (BxPC-3), breast (MDA-MB-468), epidermoid (A431), and lung (A549) cancer cell lines were from ATCC (Rockville, MD). The mouse embryonic fibroblast NIH/3T3 cell line was kindly provided by S. Schmidt (CNRS-UMR 5237, Montpellier, France). EGFR-, HER2-, HER3-, HER2/HER3-, and EGFR/HER4-transfected NIH/3T3 cell lines were obtained as previously described [32]. Cell culture was detailed in the Supplementary Materials.

### *Ab Generation*

Anti-HER3 human Ab (huAb) fragments were selected from the human scFv phage library MG-Umab [33] and expressed as fully human $IgG_1$ for further characterization. HER3-specific mouse monoclonal Abs were obtained by lymphocyte hybridization. Experiments were detailed in the Supplementary Materials.

### *Xenograft Studies*

All *in vivo* experiments were performed in compliance with the national regulations and ethical guidelines for experimental animal studies in an accredited establishment (Agreement No. C34-172-27). Six-week-old female athymic mice, purchased from Harlan (Indianapolis, IN), were injected subcutaneously into the right flank with A431 ($0.7 \times 10^6$), A549 ($10 \times 10^6$), BxPC3 ($3.5 \times 10^6$), or MDA-MB-468 ($3 \times 10^6$) cells. Tumor-bearing mice were randomized in the different treatment groups when tumors reached a minimum size of 120 $mm^3$ and were intraperitoneally treated with anti-HER3 Abs (15 mg/kg) or a combination of anti-HER3 Abs and trastuzumab (ratio 1:1; 10 mg/kg of each Ab), every 2 days for 4 or 6 weeks. Tumor dimensions were measured once or twice weekly and volumes were

calculated with the formula: $D_1 \times D_2 \times D_3/2$. Kaplan-Meier survival estimates were calculated from the date of the xenograft until the date of the event of interest and compared using the log-rank test. The event of interest was reaching a tumor volume of 2000 $mm^3$, when mice were sacrificed.

### *HER3 Binding Studies*

The binding specificity of selected Abs to soluble and membrane HER3 was assessed by ELISA, flow cytometry, and surface plasmon resonance and detailed in the Supplementary Materials.

### *Epitope Determination by SPOT Peptide Analysis*

Two hundred thirteen overlapping pentadecapeptides that were frame-shifted by one or three residues and that covered the amino acid sequence of the HER3 ECD (amino acids 1–645) were synthesized on cellulose membrane. After three washes in TBS buffer (50 mM Tris, 137 mM NaCl, 2.68 mM KCl), membranes were saturated in TBS containing 5% sucrose and casein-based blocking buffer (1:50; Sigma-Aldrich, St Louis, MO) at 25°C overnight. After three washes in TBS containing 0.05% Tween 20, cellulose-bound peptides were probed with 1 to 10 μg/ml anti-HER3 Abs in TBS containing 5% sucrose and casein-based blocking buffer and concomitantly or sequentially incubated with peroxidase-conjugated goat $F(ab)'_2$ secondary Ab (Jackson ImmunoResearch, West Grove, PA) as appropriate, at 37°C for 1.5 hours. After three washes in TBS containing 0.05% Tween 20, Ab binding was detected with the ECL Western Blotting Detection Kit (PerkinElmer, Waltham, MA).

For SPOT alanine scanning analysis, 39 pentadecapeptides corresponding to the Ab-immunoreactive amino acid sequences previously identified and the 15 alanine analogs of each peptide were synthesized by the SPOT method. Ab reactivity of cellulose-bound peptides was assayed as described above. Spot reactivity was evaluated by scanning the membranes and measuring the spot intensities with ImageJ 1.44 (http://rsbweb.nih.gov/ij). SPOT critical residues (SCR), within the HER3 epitopes recognized by the selected Abs, were identified on the basis of the Ab-binding capacity of the relevant alanine analog (at least 20% lower than that of the unmodified peptide sequence).

### *Flow Cytometry–Based NRG-Binding Competition Experiments*

Competition experiments were performed to quantify the ability of NRG to inhibit Ab binding to HER3 in an SKBR3 cell–based assay. To this end, $10^5$ SKBR3 cells were pre-incubated with various concentrations of the competing NRG ligand on ice for 1.5 hours. After one wash with phosphate-buffered saline (PBS)–1% BSA, anti–HER3 Abs were added to each well at the concentration that gives 50% of the maximal binding, on ice for 1 hour. In some experiments, NRG ligand and anti-HER3 Abs were co-incubated on ice for 2 hours and showed similar results. Cells were then washed and incubated with the appropriate fluorescein isothiocyanate (FITC)–conjugated secondary Ab (1:60 dilution; Sigma) on ice for 45 minutes, before cytometric analysis on a Quanta apparatus (Beckman Coulter, Fullerton, CA).

### *Cell Cycle, Proliferation, and Apoptosis Assays*

The effect of HER3-specific Abs on the cell cycle was evaluated using propidium iodide staining. Briefly, 300,000 BxPC3 tumor cells/well were cultured in six-well microtiter plates for 24 hours and then serum starved and synchronized in Roswell Park Memorial Institute medium (RPMI) without fetal calf serum (FCS) for another 24 hours, before co-incubation with 100 μg/ml anti-HER3 Abs and 100 ng/ml NRG. Permeabilized cells were stained 24 hours later with propidium iodide before flow cytometric analysis. For proliferation and apoptosis assays, 50,000 BxPC3 cells/well were plated 1 day before starvation (in RPMI–1% FCS). HER3-specific Abs and NRG were then added for 120 hours. Cell proliferation was measured by incorporating Alexa Fluor 488–conjugated 5-ethynyl-2′-deoxyuridine (Invitrogen, Carlsbad, CA) during the last 30 hours of culture. Cell apoptosis was assessed by incubation with fluorescence-conjugated Annexin V and 7-aminoactinomycin D (Beckman Coulter). All experiments were performed in triplicate.

### *Western Blot Analysis*

Cellular fractionation of treated BxPC3 tumor cells and further Western blot using appropriate Abs were detailed in the Supplementary Materials.

### *Homogeneous Time-resolved Fluorescence (HTRF) Analysis of HER2/HER3 Heterodimerization*

HER2/HER3 heterodimers were quantified using Ab-based time-resolved fluorescence resonance energy transfer (TR-FRET) assay, as previously described [32] and detailed in the Supplementary Materials.

### *Statistical Analysis*

A linear mixed regression model was used to determine the relationship between tumor growth and the number of days post-graft. The fixed part of the model included variables corresponding to the number of days post-graft and the different groups. Interaction terms were built into the model. Random intercept and random slope were included to take into account the time effect. The coefficients of the model were estimated by maximum likelihood and considered significant at the 0.05 level. Survival rates were estimated from the date of the xenograft until the date when the tumor reached a volume of 2000 $mm^3$ using the Kaplan-Meier method. Median survival was presented with 95% confidence intervals. Survival curves were compared using the log-rank test. Statistical analyses were carried out using the STATA 11.0 software (StataCorp, College Station, TX).

## Results

### *Selected Anti-HER3 Abs Bind to the Extracellular Region of Human HER3 but Not to the Other HER Receptors*

Of the approximately 1000 mouse hybridomas screened, 10 mouse Abs (moAbs) recognized the ECD of human HER3 but not mouse HER3 (Figure 1*A*) or the other HER family members (Figure 1*B*) in ELISA or flow cytometry assays. Among the 144 individual phage-infected colonies selected from the human scFv library MG-Umab [33], nine huAbs, expressed as fully human $IgG_1$, specifically bound to human HER3 (Figure 1*A*) but not to other human HER receptors (Figure 1*B*) and six cross-reacted with mouse HER3 (Figure 1*A*). The selected huAbs and moAbs targeted soluble human HER3 (Figure 1*A*) and membrane-anchored HER3 in NIH/3T3 cells that express HER3 alone or together with HER2 (HER2/HER3) (Figure 1*B*). Surface

A

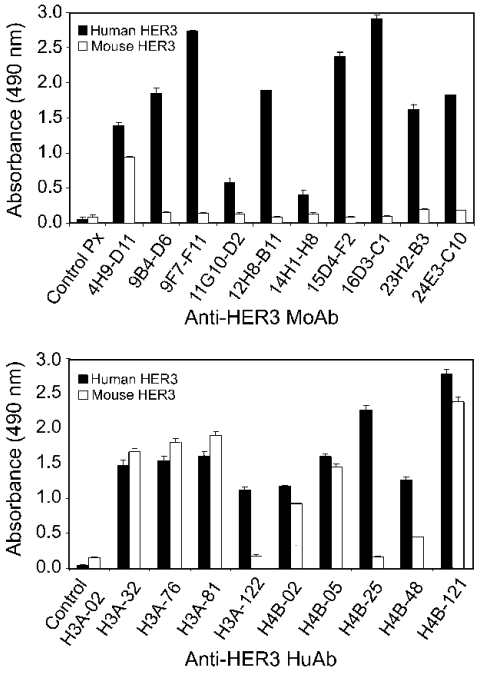


B

| Antibody | Parental 3T3 cells | Transfected 3T3 cells | | | | |
|---|---|---|---|---|---|---|
| | | EGFR | HER2 | HER3 | HER2/HER3 | EGFR/HER4 |
| HER3-specific HuAbs | | | | | | |
| Anti-human 2nd Ab | 0.3 | 0.2 | 0.4 | 0.3 | 0.5 | 0.5 |
| Control H3A-02 | 0.4 | 0.2 | 0.5 | 0.5 | 0.5 | 0.6 |
| H3A-32 | 0.5 | 0.3 | 0.4 | 10.5 | 68.8 | 0.5 |
| H3A-76 | 0.6 | 0.2 | 0.5 | 11.5 | 66.6 | 0.5 |
| H3A-81 | 0.6 | 0.3 | 0.5 | 10.6 | 68.5 | 0.5 |
| H3A-122 | 1.3 | 0.3 | 0.9 | 6.6 | 35.0 | 0.6 |
| H4B-02 | 0.5 | 0.3 | 0.4 | 7.9 | 13.3 | 0.5 |
| H4B-05 | 0.5 | 0.3 | 0.4 | 7.9 | 13.3 | 0.5 |
| H4B-25 | 0.8 | 0.3 | 0.7 | 5.1 | 37.8 | 0.7 |
| H4B-48 | 1.0 | 0.6 | 1.1 | 7.5 | 27.5 | 1.2 |
| H4B-121 | 0.7 | 0.3 | 0.6 | 12.3 | 70.4 | 0.7 |
| HER3-specific MoAbs | | | | | | |
| Anti-mouse 2nd Ab | 0.3 | 0.4 | 0.4 | 0.3 | 0.3 | 0.3 |
| Control Px | 0.5 | 0.3 | 0.6 | 0.4 | 0.5 | 0.6 |
| 4H9-D11 | 0.3 | 0.3 | 0.3 | 0.7 | 1.3 | nd |
| 9B4-D6 | 0.2 | 0.2 | 0.3 | 6.6 | 18.3 | nd |
| 9F7-F11 | 0.3 | 0.4 | 0.4 | 1.8 | 12.4 | 0.3 |
| 11G10-D2 | 0.3 | 0.2 | 0.3 | 1.4 | 10.1 | nd |
| 12H8-B11 | 0.3 | 0.4 | 0.5 | 3.7 | 28.8 | 0.3 |
| 14H1-H8 | 0.4 | 0.4 | 0.5 | 0.9 | 1.1 | nd |
| 15D4-F2 | 0.4 | 0.3 | 0.4 | 4.2 | 25.6 | nd |
| 16D3-C1 | 0.4 | 0.4 | 0.7 | 4.5 | 26.8 | 0.3 |

C

| Antibody | $k_a$ $M^{-1}$ $s^{-1}$ | $k_d$ $s^{-1}$ | $K_D$ nM |
|---|---|---|---|
| HER3-specific HuAbs | | | |
| H3A-122 | $2.0 \times 10^5$ | $2.1 \times 10^{-3}$ | 10.4 |
| H4B-25 | $8.8 \times 10^4$ | $7.2 \times 10^{-2}$ | 221.0 |
| H4B-121 | $1.2 \times 10^5$ | $3.2 \times 10^{-3}$ | 26.1 |
| HER3-specific MoAbs | | | |
| 9F7-F11 | $5.4 \times 10^4$ | $2.4 \times 10^{-4}$ | 4.4 |
| 11G10-D2 | $3.5 \times 10^5$ | $7.9 \times 10^{-3}$ | 22.6 |
| 12H8-B11 | $6.6 \times 10^4$ | $1.6 \times 10^{-4}$ | 2.4 |
| 14H1-H8 | $1.3 \times 10^5$ | $4.0 \times 10^{-3}$ | 30.7 |
| 15D4-F2 | $2.3 \times 10^5$ | $1.4 \times 10^{-2}$ | 63.7 |
| 16D3-C1 | $8.7 \times 10^4$ | $8.9 \times 10^{-5}$ | 1.0 |

D

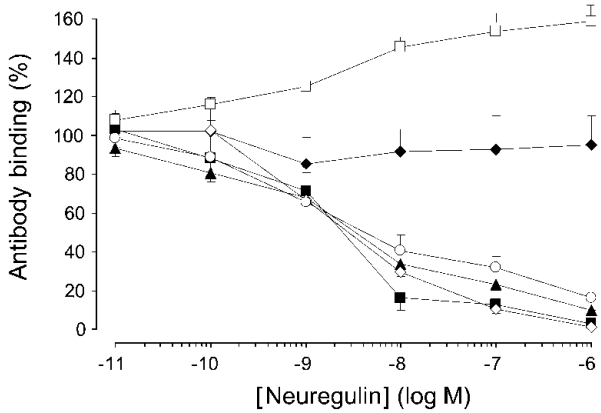


**Figure 1.** Selected anti-HER3 Abs bind to the extracellular region of human HER3 but not to the other HER receptors, with or without interference with NRG binding. (A) Cross-reactivity of anti-HER3 moAbs and huAbs toward mouse or human soluble HER3 was assessed by ELISAs. The absorbance values at 490 nm of the irrelevant control Abs Px and H3A-02 are indicated. Each value represents the mean ± SD of triplicate determinations in three independent experiments. (B) Flow cytometric analysis of the anti-HER3 Ab binding to NIH/3T3 fibroblasts transfected with membrane EGFR, HER2, HER3, HER2/HER3, or EGFR/HER4 in comparison to parental NIH/3T3 cells. Binding of the FITC-conjugated secondary Abs and of the control Abs H3A-02 and Px is also indicated. Results (geometric mean) are representative of two different experiments. (C) BiaCore determination of the binding kinetics between anti-HER3 huAbs and recombinant human HER3 (3.12–6.25 nM) and between moAbs and human HER3 (extracellular)–Fc recombinant protein (77 nM), respectively. (D) NRG interference with anti-HER3 Ab binding in HER3-positive SKBR3 cells was determined by competitive flow cytometry. The binding (%) of the moAbs 9F7-F11 (□), 16D3-C1 (○), and 12H8-B11 (◇), and of the huAbs H4B-121 (▲), H3A-122 (■), and H4B-25 (♦) to SKBR3 cells, after incubation with various NRG concentrations, is indicated. Each value represents the mean ± SD of triplicate determinations in three independent experiments. No cell binding was observed when only the FITC-conjugated secondary Ab was added after incubation with NRG.

plasmon resonance (Figure 1*C*) showed that the huAbs H3A-122 and H4B-121 and the moAbs 9F7-F11, 12H8-B11, and 16D3-C1 had the best affinities (nanomolar range). The association rate ($k_a$) for these Abs ranged between $5 \times 10^4$ and $1 \times 10^5$ $M^{-1}$ $s^{-1}$, whereas their dissociation rate ($k_d$) was between $1 \times 10^{-3}$ and $1 \times 10^{-4}$ $s^{-1}$. Competition experiments by flow cytometry demonstrated that moAb 9F7-F11 and huAb H4B-25 did not compete with NRG, thus suggesting that these Abs do not bind to the NRG-binding site (Figure 1*D*). Incubation of SKBR3 cells with $10^{-11}$ to $10^{-6}$ M NRG led to a ligand-dependent increase of 9F7-F11 binding to HER3. In contrast, the moAbs 12H8-B11 and

16D3-C1 as well as the huAbs H3A-122 and H4B-121 showed an NRG-dependent decrease in binding to HER3, indicating that the epitopes recognized by these Abs are close to the NRG-binding site (Figure 1*D*). The NRG concentration that inhibited 50% binding ranged between 2.5 and 4 nM.

### *Anti-HER3 Abs Target Epitopes that Are Located in Domain 1, 3, or 4 of HER3*

To identify the motifs recognized by the selected anti-HER3 Abs, we used the SPOT method to synthesize 213 cellulose membrane-bound pentadecapeptides that cover the entire ECD of human HER3. Epitopes in D3 were recognized by the huAbs H4B-121 (amino acids 342–358; Figure 2*A*) and H4B-25 (residues 460–477), and H3A-122 bound to an epitope in D4 (amino acids 495–510). In contrast, the moAbs 9F7-F11 and 16D3-C1 showed reactivity toward D1 sequences (amino acids 37–51 and 112–128, respectively; data not shown). Alanine analogs of the 39 pentadecapeptides that corresponded to the Ab-binding sequences were then synthesized using the SPOT method to identify the HER3 residues that are critically involved in Ab binding (SCRs; see Figure 2, *B* and *C*, for an example). In summary, the alanine scanning experiments indicated that the key binding motif for H4B-121 on D3 is $^{352}$DPWHKI$^{358}$ and that Asp$^{352}$, Trp$^{354}$, His$^{355}$, and Lys$^{356}$ are the main SCRs. Moreover, the observation that Trp$^{354}$, His$^{355}$, and Lys$^{356}$ in $^{352}$DPWHKI$^{358}$ are phylogenetically conserved in mouse and monkey HER3 (Figure 3*B*) explains why H4B-121 bound to both human and mouse HER3 in ELISAs and suggests that H4B-121 might cross-react also with rhesus monkey HER3 (*Macaca mulatta*). Conversely, the lack of sequence conservation with human EGFR, HER2, and HER4 explains why H4B-121 did not recognize other HER family receptors in flow cytometry assays. The motif $^{469}$RPRR-VA$^{476}$ in D3 was found to be critical for binding of H4B-25 Ab and residues Arg$^{471}$, Arg$^{472}$, and Val$^{475}$ were the main SCRs (Figure 3*A*). Two SCRs (Arg$^{471}$ and Arg$^{472}$) and also Asp$^{473}$ are not conserved in mouse HER3 or in human EGFR, HER2, and HER4 (Figure 3*B*), consistent with the absence of cross-reaction for this Ab in ELISA and flow cytometric assays. However, as the $^{469}$RPRR-VA$^{476}$ binding motif is conserved in monkey HER3, the H4B-25 Ab might recognize monkey HER3. The $^{502}$RNY-R$^{506}$ sequence in D4 was identified as the binding motif for H3A-122 and residues Tyr$^{504}$ and Arg$^{506}$ as the main SCRs (Figure 3*A*). This motif is conserved in the human and monkey HER3 sequences (Figure 3*B*) but not in those of other HER family members (particularly the SCR Tyr$^{504}$), thus explaining the absence of cross-reaction with other human HER family members (Figure 1, *A* and *B*). Alanine scanning of pentadecapeptides in D1 identified $^{112}$L-LT-LTEILS$^{122}$ as the binding motif for 16D3-C1 and Leu$^{120}$, Glu$^{122}$, Ile$^{123}$, and Leu$^{124}$ as the main SCRs (Figure 3*A*). The amino acid difference at positions 114 and 125 might explain why 16D3-C1 did not bind to mouse HER3. The Ab 9F7-F11 recognized the motif $^{44}$LEIVL$^{48}$ in D1 and residues Leu$^{44}$, Ile$^{46}$, and Leu$^{48}$ were identified as SCRs (Figure 3*A*). The $^{112}$L-LT-LTEILS$^{122}$ (16D3-C1) and $^{44}$LEIVL$^{48}$ (9F7-F11) sequences are not conserved in other HER family receptors (Figure 3*B*), explaining why these Abs did not cross-react with EGFR, HER2, or EGFR/HER4. In contrast, the complete sequence homology with monkey HER3 suggests that these Abs might cross-react with monkey HER3 (Figure 3*B*). We then positioned the SCRs of each binding motif on the crystallographic structure of unliganded HER3 (pdb 1M6B; Figure 3*C*). The H4B-121 binding motif $^{352}$DPWHKI$^{358}$ protruded at the junction between D2 and D3, whereas $^{469}$RPRR-VA$^{476}$ (H4B-25) was close to the C terminus of D3 and $^{502}$RNY-R$^{506}$ (H3A-122) was at the N terminus of D4. These two binding motifs are opposite to the H4B-121 epitope. The H4B-25 binding motif, which is involved in an α-helix structure, was within a "hot-spot" region and overlapped with the HER3 epitope recognized by the "two-in-one" EGFR/HER3 Ab MEHD7945A [27]. Moreover, it included amino acid positions that align with residues that are critically involved in the binding of MEHD7945A [27], matuzumab [31], nimotuzumab [34], and cetuximab [35] to EGFR. The 9F7-F11 epitope $^{44}$LEIVL$^{48}$ was located in one of the prominent β-strands at the beginning of D1, facing the H4B-121 epitope at a distance of 60 Å across D2. The 16D3-C1 binding motif $^{112}$L-LT-LTEILS$^{122}$ was deeply located inside the β-strand structure of D1.

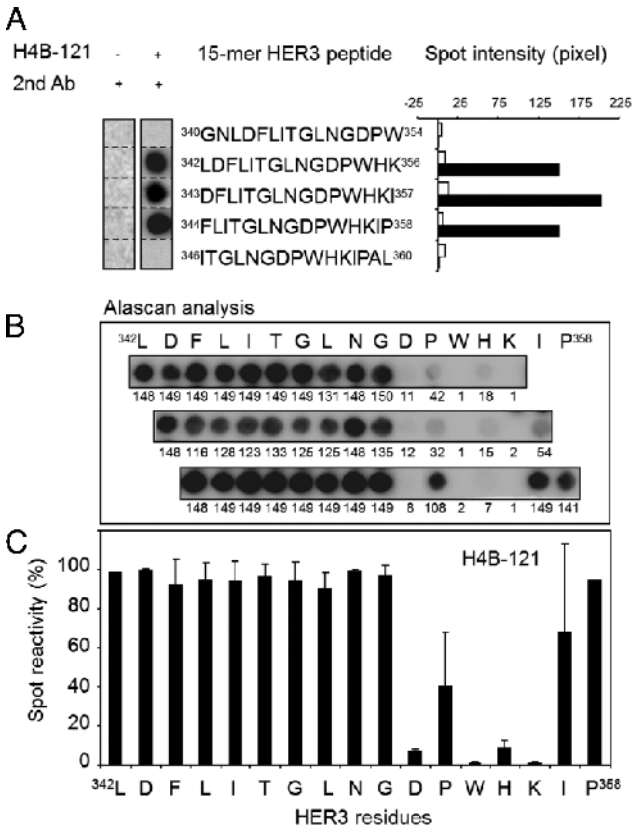


**Figure 2.** The $^{352}$DPWHKI$^{358}$ motif recognized by the Ab H4B-121 is located in D3 of HER3. (A) Scan analysis of the 213 overlapping pentadecapeptides that covered the entire extracellular domain of HER3 (amino acids 1–645) and were frame-shifted by one or three residues (generated by the SPOT method). Binding of H4B-121 was observed only in the region between amino acids 340 and 360. No binding was observed with the secondary Ab alone. The Spot intensity was measured using ImageJ. (B) Alanine scanning (Alascan) of the pentadecapeptides $^{342}$LDFLITGLNGDPWHK$^{356}$, $^{343}$DFLITGLNGDPWHKI$^{357}$, and $^{344}$FLITGLNGDPWHKIP$^{358}$ that cover the region between amino acids 342 and 358 of HER3. (C) Quantitative analysis of H4B-121 binding to the membrane pentadecapeptides in B using ImageJ. Each bar represents the reactivity of H4B-121 toward a pentadecapeptide sequence in which the indicated amino acid was substituted by alanine. The mean spot reactivity for each residue was calculated from the results obtained in the three pentadecapeptides.

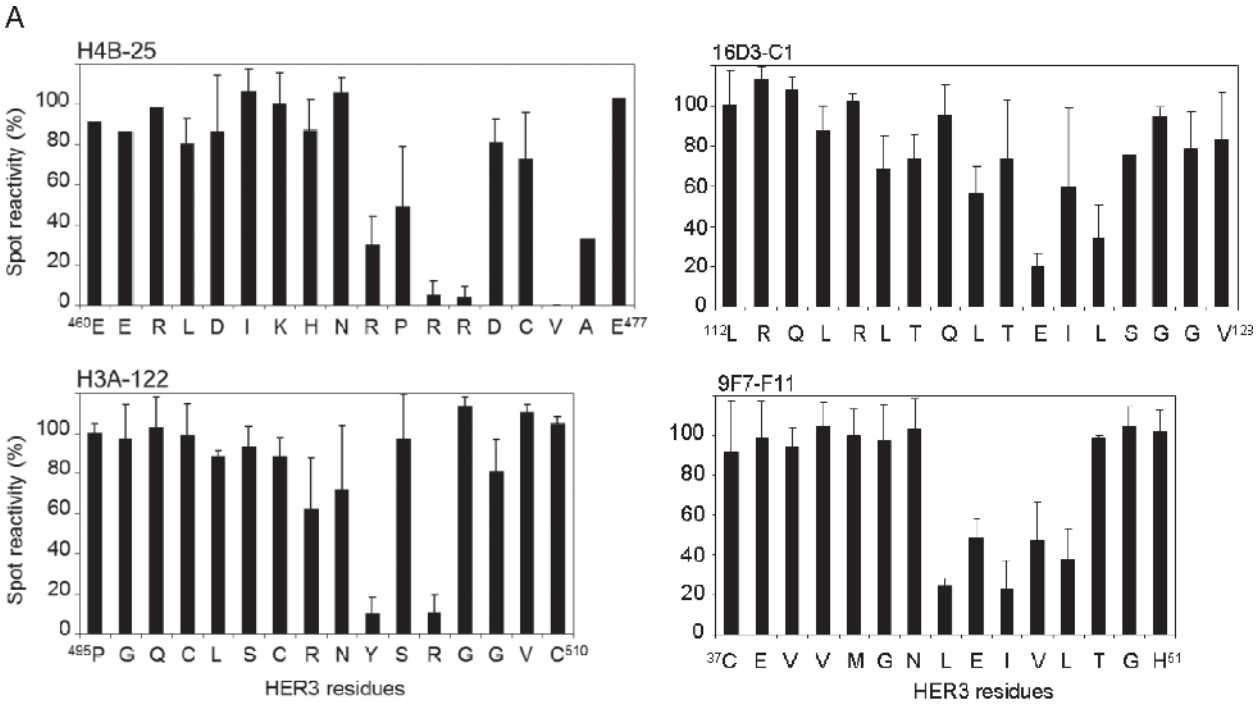


B

H4B-121 epitope

| | 352 | | | | | 357 |
|---|---|---|---|---|---|---|
| Human HER3 | D | P | W | H | K | I |
| Monkey HER3 | — | — | — | — | — | — |
| Mouse HER3 | — | — | — | — | — | — |
| Human EGFR | — | S | F | T | H | T |
| Human HER2 | — | — | A | S | N | T |
| Human HER4 | — | — | Y | N | A | — |

H4B-25 epitope

| | 469 | | | | | | | 476 |
|---|---|---|---|---|---|---|---|---|
| Human HER3 | R | P | R | R | D | C | V | A |
| Monkey HER3 | — | — | — | — | — | — | — | — |
| Mouse HER3 | — | — | L | G | E | — | — | — |
| Human EGFR | — | G | E | N | S | — | K | — |
| Human HER2 | — | — | E | D | E | — | — | G |
| Human HER4 | — | K | A | E | N | — | T | — |

H3A-122 epitope

| | 502 | | | | 506 |
|---|---|---|---|---|---|
| Human HER3 | R | N | Y | S | R |
| Monkey HER3 | — | — | — | — | — |
| Mouse HER3 | — | — | — | — | — |
| Human EGFR | — | — | V | — | — |
| Human HER2 | S | Q | F | L | — |
| Human HER4 | — | R | F | — | — |

9F7-F11 epitope

| | 44 | | | | 48 |
|---|---|---|---|---|---|
| Human HER3 | L | E | I | V | L |
| Monkey HER3 | — | — | — | — | — |
| Mouse HER3 | — | — | — | — | — |
| Human EGFR | — | — | — | T | Y |
| Human HER2 | — | — | L | T | Y |
| Human HER4 | — | — | — | T | S |

16D3-C1 epitope

| | 112 | | | | | | | | | | 122 |
|---|---|---|---|---|---|---|---|---|---|---|---|
| Human HER3 | L | R | L | T | Q | L | T | E | I | L | S |
| Monkey HER3 | — | — | — | — | — | — | — | — | — | — | — |
| Mouse HER3 | — | — | F | — | — | — | — | — | — | — | L |
| Human EGFR | — | P | M | R | N | — | Q | — | — | — | H |
| Human HER2 | — | Q | — | R | S | — | — | — | — | — | K |
| Human HER4 | — | G | — | K | N | — | — | — | — | — | N |

C

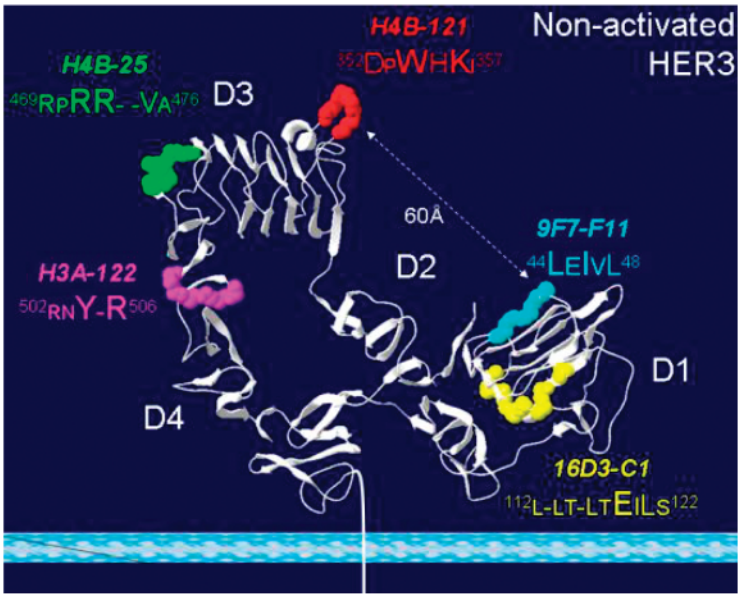


**Figure 3.** The Abs H4B-25 and H3A-122 recognize motifs located in D3 and D4, respectively, whereas the Abs 16D3-C1 and 9F7-F11 bind to motifs within D1 of HER3. (A) Quantitative analysis of the reactivity of H4B-25, H3A-122, 16D3-C1, and 9F7-F11 toward pentadecapeptides generated by SPOT synthesis on cellulose membranes using ImageJ. (B) Amino acid alignment of the identified Ab-binding motifs in human, monkey, and mouse HER3 and in human EGFR, HER2, and HER4. (C) The Ab-binding motifs were localized on the crystal structure of unliganded HER3 (pdb 1M6B).

### *The D1-Specific Abs 16D3-C1 and 9F7-F11 and the D3-specific Ab H4B-121 Reduce Tumor Growth in Mice Xenografted with Tumor Cells with Different Biologic Profiles*

To assess the anti-tumor activity of selected anti-HER3 Abs *in vivo*, we first xenografted subcutaneously nude mice with *HER2* non-amplified BxPC3 pancreatic cancer cells that express HER3 at low level (between 10,000 and 20,000 receptors/cell). When tumors reached a volume of 120 $mm^3$, mice ($n$ = 8/each condition) were treated with 15 mg/kg anti-HER3 Ab 16D3-C1, 9F7-F11, or H4B-121, as single agents, every 2 days for 6 weeks. At day 56 post-xenograft (corresponding to day 26 of the Ab treatment), mean tumor volume was significantly smaller (68 ± 4% reduction; $P < .001$) in Ab-treated mice than in mice treated with vehicle (controls; Figure 4*A*, *left panel*). At the end of the experiment (160 days), Kaplan-Meier analysis revealed that the 50% median survival time was significantly delayed by 18 days in mice treated with the anti-HER3 Abs 9F7-F11 and H4B-121 (Figure 4*A*, *right panel*) and by 24 days (and one mice was completely cured) in mice treated with 16D3-C1 in comparison to controls ($P < .001$). Analysis of tumor samples at day 24 of treatment showed that HER3 phosphorylation at $Tyr^{1289}$ was inhibited and HER3 was down-regulated in Ab-treated mice in comparison to vehicle-treated mice (Figure 4*B*).

We next used these Abs to treat mice that had been xenografted with NRG-addicted epidermoid A431 tumor cells [17] or triple-negative breast cancer MDA-MB-468 cells. *HER2* non-amplified ($HER^{low}$) epidermoid A431 cells secrete the HER3 ligand NRG [17] and express around 10,000 HER3 receptors per cell, whereas MDA-MB-468 cells also express HER3 at low level (around 6000 to 8000 receptors per cell) and harbor mutant *PTEN*. As observed in mice xenografted with BxPC3 cancer cells, mean tumor volume was significantly lower in Ab-treated mice xenografted with A431 cells (53 ± 6% reduction; $n$ = 8 animals/condition) at day 31 post-xenograft (20 days after the beginning of the treatment; Figure 4*C*, *left panel*; $P < .001$) or with MDA-MB-468 cells (35% and 40% volume reduction at day 105 post-xenograft following treatment with 9F7-F11 and H4B-121, respectively; Figure 4*D*, *left panel*; $P < .05$) than in controls (vehicle). Treatment with the 16D3-C1 and 9F7-F11 Abs significantly delayed the 50% median survival time by 21 days in mice xenografted with A431 cells (one mouse cured for both Ab groups at the end of the experiment, i.e., 140 days; $P < .001$; Figure 4*C*, *right panel*) and by 20 days in animals xenografted with MDA-MB-468 cells (one mouse was stabilized for both Ab groups at the end of the experiment, i.e., 190 days; $P < .05$; Figure 4*D*, *right panel*). Treatment with the Ab H4B-121 delayed the median survival time by 14 days in animals xenografted with A431 cells (Figure 4*C*, *right panel*; $P < .01$) and by 61 days in mice xenografted with MDA-MB-468 cells (three mice were stabilized at the end of the experiment, i.e., 190 days; $P < .01$; Figure 4*D*, *right panel*). Taken together, these results demonstrate that anti–HER3 D1 and D3 Abs delay tumor growth in mice xenografted with different cancer cell lines, irrespectively of their biologic profile (i.e., NRG addiction and HER2 status).

### *Combined Treatment with the Anti-HER3 Ab 16D3-C1 and Trastuzumab Improves Inhibition of $HER2^{low}$ Tumor Growth in Nude Mice*

We previously demonstrated that the combination of anti-HER2 trastuzumab with anti-EGFR therapy has a synergistic anti-cancer effect in mice xenografted with $HER2^{low}$ pancreatic carcinoma cells [36]. To assess the effect on $HER2^{low}$ tumor xenografts of combined treatment with trastuzumab and the anti-HER3 Ab 16D3-C1, we xenografted mice ($n$ = 8/each condition) with $HER2^{low}$ epidermoid A431 or lung A549 cancer cells. Both cell lines secrete NRG [17,37] and show no [38] or moderate [39] response to trastuzumab therapy, respectively. To highlight a potential synergistic effect, sub-efficient doses of 16D3-C1 and trastuzumab (10 mg/kg every 2 days for 4 weeks) were administered. Tumor growth was significantly reduced (60% in A431 cell xenografts and 75% in A549 cell xenografts) in mice treated with both Abs ($P < .001$) at day 35 post-xenograft in comparison to mice treated with 16D3-C1 alone (25% reduction in A431 and 50% reduction in A549 xenografts) or with trastuzumab alone or vehicle (no reduction; Figure 5). These results demonstrate that the combination of an HER3-specific Ab and trastuzumab might be effective in $HER2^{low}$ carcinomas that secrete NRG.

### *Anti-HER3 Abs Induce Cell Cycle Arrest in $G_1$ Phase, Leading to Proliferation Inhibition and Apoptosis of Pancreatic BxPC3 Cancer Cells*

As our anti–HER3 D1 and D3 Abs efficiently inhibited tumor growth *in vivo* alone or in combination with trastuzumab, we then investigated *in vitro* their effects on cell cycle, proliferation, and apoptosis. Exposure of NRG-stimulated BxPC3 pancreatic cancer cells to the Abs 9F7-F11 and 16D3-C1 for 24 hours induced cell cycle arrest in $G_1$ phase (particularly in cells incubated with 9F7-F11), leading to a lower number of cells in S and $G_2$/M phases in comparison to untreated cells or cells incubated with the irrelevant Px Ab (controls; Figure 6*A*). An anti-proliferative effect of the three anti-HER3 Abs was observed at 120-hour post-incubation (Figure 6*B*). Moreover, early and late apoptosis of ligand-stimulated BxPC3 cells was also observed upon exposure to HER3-specific Abs 9F7-F11 and 16D3-C1 (Figure 6*C*). These results indicate that anti-HER3 Abs induce cell cycle arrest, leading to subsequent proliferation inhibition and apoptosis, in agreement with their inhibition of tumor growth *in vivo*.

### *The Abs 16D3-C1, 9F7-F11, and H4B-121 Block HER2/HER3 Dimerization*

Members of the HER family modulate their downstream signaling and oncogenic effects through receptor homodimerization and heterodimerization. Using a recently described Ab-based TR-FRET assay [32], we assessed whether our HER3-specific Abs could block HER2/HER3 heterodimerization in NIH/3T3 cells that express both HER2 and HER3. These cells were chosen because 1) they express more HER3 receptors (946,000/cell) than HER2 receptors (126,000/cell), thus allowing a better fluorescence signal to follow heterodimer formation, and 2) they were sensitive to the inhibitory effects of HER3 Abs in a cell proliferation assay (24 ± 6% inhibition with 16D3-C1, 32 ± 9% with 9F7-F11, and 22 ± 1% with H4B-121, respectively). In the absence of exogenous NRG stimulation, a significant dose-dependent disruption of HER2/HER3 heterodimers was observed when cells were incubated with the Abs 16D3-C1 and 9F7-F11 (around 30%) or H4B-121 (38%) in comparison to untreated cells (Figure 7; $P < .001$). Trastuzumab treatment also blocked HER2/HER3 heterodimerization in a dose-dependent way in these cells. Conversely, incubation with exogenous NRG increased HER2/HER3 formation (up to 60%), as expected [5]. Pre-incubation

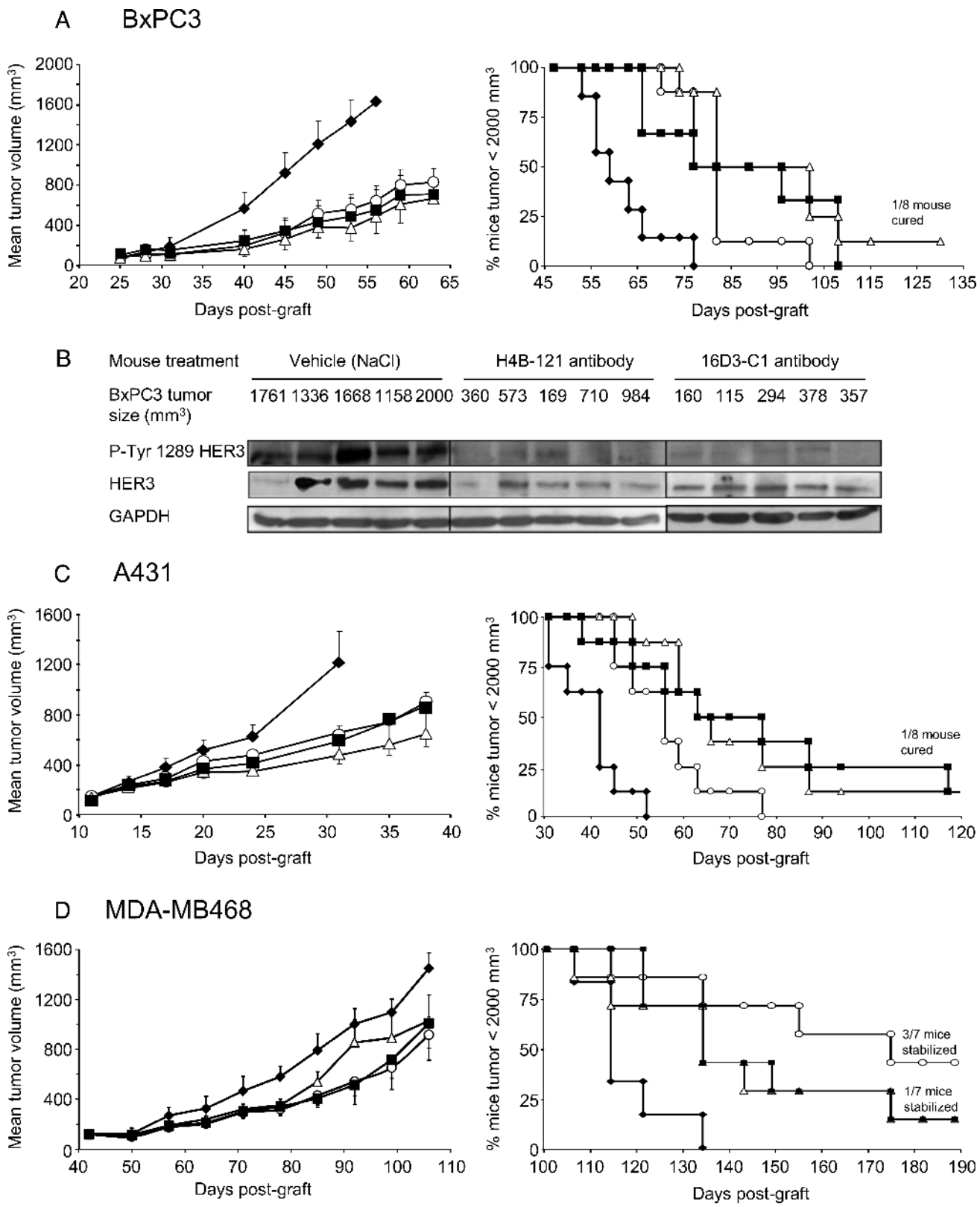


**Figure 4.** The anti–HER3 D1 Abs 9F7-F11 (■) and 16D3-C1 (▵) and the anti-HER3 D3 Ab H4B-121 (○) inhibit tumor growth (left panel) and increase survival time (right panel) compared to vehicle (NaCl; ♦) in mice xenografted with *HER2* non-amplified pancreatic carcinoma BxPC3 cells (wild-type *PIK3CA* and *p53*) (A), NRG-addicted, *HER2* non-amplified epidermoid carcinoma A431 cells (wild-type *PIK3CA* and mutant *p53*) (C), or triple-negative, *EGFR*-amplified breast carcinoma MDA-MB-468 cells (wild-type *PIK3CA* and mutant *p53*) (D). BxPC3 tumor lysates from vehicle- or Ab-treated mice were prepared 24 days after the beginning of the treatment (tumor sizes are indicated) and HER3 phosphorylation at $Tyr^{1289}$ was assessed by Western blot analysis (B). Tumor growth data are presented as the mean tumor volume ± SEM for each group of nude mice ($n = 8$ per condition, but for the MDA-MB-468 xenograft model, $n = 7$). Kaplan-Meier survival curves were calculated when tumors reached a volume of 2000 $mm^3$ and mice were sacrificed.

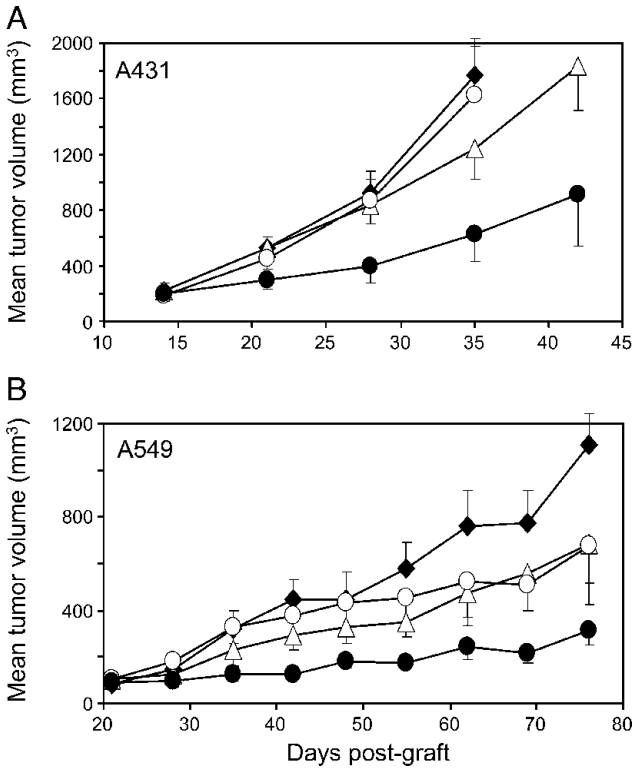


**Figure 5.** Dual treatment with the anti–HER3 D1 Ab 16D3-C1 and trastuzumab (●) improves tumor growth inhibition in nude mice xenografted with $HER2^{low}$ A431 epidermoid (A) or A549 lung (B) carcinoma cells in comparison to mice treated with vehicle (NaCl; ♦), 16D3-C1 (△) or trastuzumab (○) alone. Tumor growth data are presented as the mean tumor volume ± SEM for each group of eight nude mice.

with the control Ab Px did not influence HER2/HER3 dimer formation (Figure 7). Finally, HER3-specific Abs did not modify HER2 and HER3 expression (data not shown). Taken together, these results indicate that anti-HER3 Abs act by disrupting HER2/HER3 heterodimerization at the cell membrane.

### *The Abs 16D3-C1, 9F7-F11, and H4B-121 Inhibit HER2/HER3 Phosphorylation, Leading to Blockade of AKT-Induced Phosphorylation of Apoptosis- and Proliferation-Related Signaling Proteins*

We next evaluated the effect on downstream cell signaling of the NRG antagonist Abs 16D3-C1 and H4B-121 and of the NRG-independent Ab 9F7-F11. To this end, we used the pancreatic BxPC3 cancer cell line in which NRG potently activates the HER2/HER3 pathway. The D1-specific Ab 9F7-F11 blocked ligand-induced phosphorylation at various Tyr residues of HER2 and HER3 (Figure 8*A*). Particularly, 9F7-F11 inhibited HER3 phosphorylation at $Tyr^{1289}$, which showed no basal activation, and at $Tyr^{1262}$, which demonstrated high basal activation. $Tyr^{1289}$ HER3 interference was also observed, but at a lower level, with the NRG antagonist Abs 16D3-C1 and H4B-121. Moreover, short incubation (15 minutes) with 16D3-C1, 9F7-F11, or H4B-121 also inhibited AKT phosphorylation on $Ser^{473}$ and $Thr^{308}$ as well as phosphorylation of AKT downstream targets, such as the S6 ribosomal protein (which regulates protein translation), GSK3 (which regulates cell cycle and cell proliferation), FoxO1 and XIAP (which modulate apoptosis and cell survival), and MDM2 (which regulates p53 degradation; Figure 8*A*). We then investigated whether the anti-HER3 Abs could downregulate HER3 expression in BxPC3 cells. Short-time incubation (15 minutes) at 37°C did not induce receptor down-regulation. In contrast, 1- to 2-hour exposure at 37°C strongly reduced, in a time-dependent manner, HER3 expression, as indicated by Western blot quantification. Ab-induced HER3 down-regulation was abrogated when cells were incubated at 4°C (Figure 8*B*), thus suggesting that HER3-specific Abs promote HER3 internalization and degradation.

## Discussion

Therapeutic inhibitors of tyrosine kinase receptors that directly rely on the PI3K/AKT pathway, such as HER3, should affect proteins that regulate apoptosis and cell survival and also factors involved in compensatory signaling and drug resistance. Here, we provide evidence that anti–HER3 D1 and D3 Abs inhibit *in vivo* tumor growth by reducing HER2/HER3 dimerization and phosphorylation and, as a consequence, phosphorylation of AKT and AKT downstream targets, such as XIAP, MDM2, and FoxO1. The anti–HER3 D1 and D3 Abs showed comparable high anti-tumor activity independently of the triple-negative status (MDA-MB-468 breast cancer cells) and NRG addiction (epidermoid A431 cells and A549 lung carcinoma cells) of the xenografted cancer cell lines and also in BxPC3 xenografts. BxPC3 cells were derived from a pancreatic adenocarcinoma, a type of cancer for which very few therapeutic options (and with very modest effects) are available at the moment.

The increased anti-cancer activity of the trastuzumab/anti-HER3 Ab combination in tumor xenografts of $HER2^{low}$ cancer cells (in which trastuzumab alone shows no or low efficacy) could open new indications for anti-HER3 therapies, in addition to $HER2^{high}$ [27,29,40] and $EGFR^{high}$ [25,27] tumors. The main rationale for these combinations is that HER3 overexpression is triggered by monotreatment with EGFR- and HER2-specific Abs or small kinase inhibitors, thus allowing compensatory oncogenic signaling and cell resistance [20,25] that could be overcome with a dual therapy, as demonstrated for the EGFR-targeted therapy/anti-HER3 Ab combination in a mouse model of lung cancer [25]. Our data indicate that the anti-HER3 Ab/trastuzumab combination might represent an option for bypassing trastuzumab-induced resistance in *HER2*-amplified cancer but also for targeting $HER2^{low}$ cancer. Moreover, the synergistic effect of two HER3-specific Abs (e.g., NRG antagonism for Ab 16D3-C1 or H4B-121 and NRG-independent binding for Ab 9F7-F11), or a combination of anti-HER3 Abs plus chemotherapy [27] or radiotherapy [41], could be also envisaged to more efficiently block NRG-addicted as well as NRG-independent HER3-positive tumors.

We obtained mouse and human D1-, D3- and D4-specific Abs that can interfere or not with ligand binding. The alanine scanning analysis shows that, although charged and aromatic residues are both critical for HER3 binding by our Abs (e.g., $Asp^{352}$, $Trp^{354}$, $His^{355}$, and $Lys^{356}$ for H4B-121), non-polar aliphatic residues are also involved in HER3 binding, particularly of 9F7-F11 and 16D3-C1 (e.g., $Leu^{120}$, $Ile^{123}$, and $Leu^{124}$). As the motifs recognized by the 9F7-F11 and H4B-121 Abs overshadow the hidden D2 domain, the NRG-independent 9F7-F11 Ab might limit the NRG-induced intramolecular and intermolecular flexibility of HER3, as was suggested for zalutumumab (specific for EGFR D3), whereas the NRG antagonist H4B-121 and 16D3-C1 Abs might occlude the ligand-binding

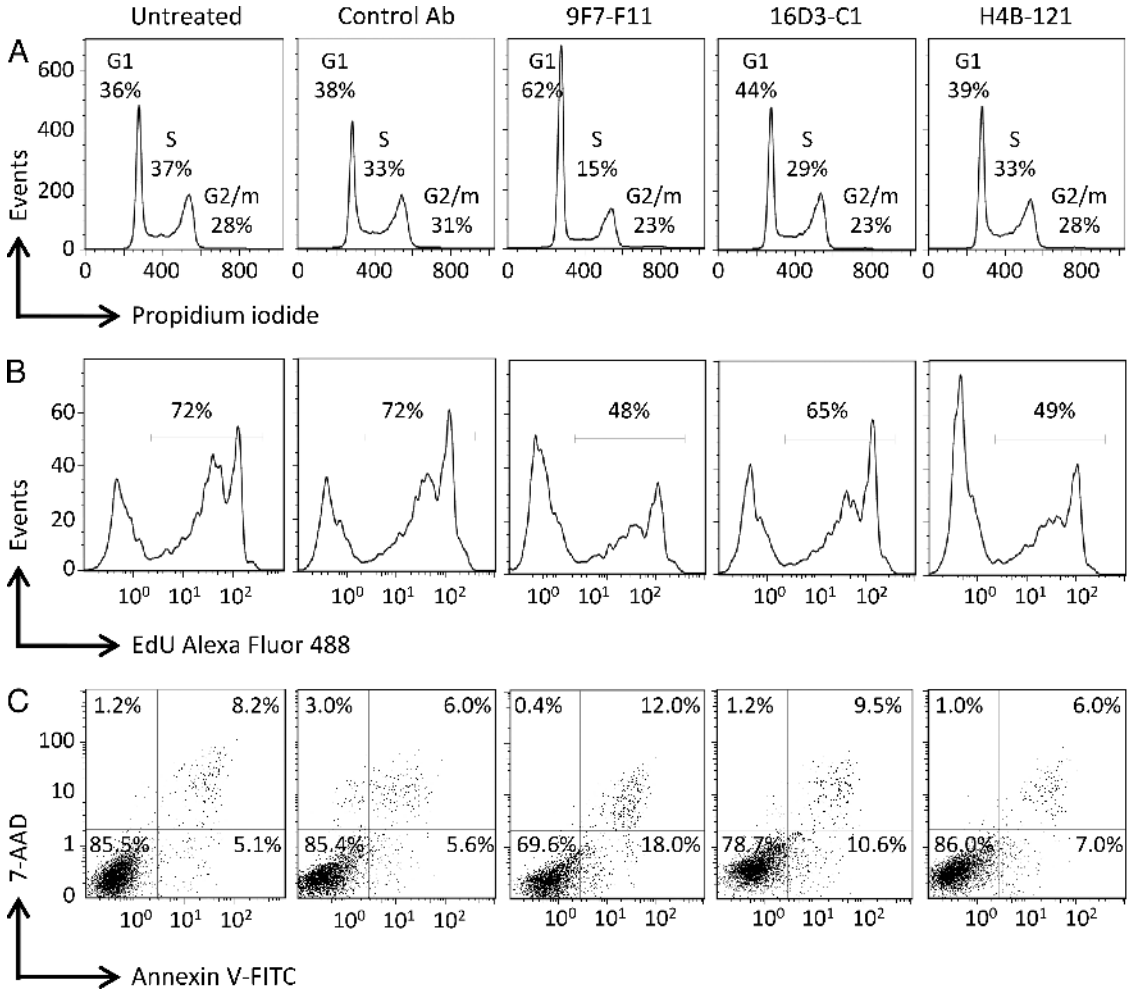


**Figure 6.** The anti-HER3 Abs block NRG-stimulated BxPC3 pancreatic cancer cells in the $G_1$ phase of the cell cycle (A), inhibit their proliferation (B), and promote cell apoptosis (C). Cell cycle progression was analyzed using propidium iodide staining; cell proliferation was quantified on the basis of the cell incorporation of Alexa Fluor 488–conjugated 5-ethynyl-2′-deoxyuridine, and apoptosis was demonstrated by staining with Annexin V and 7-aminoactinomycin D.

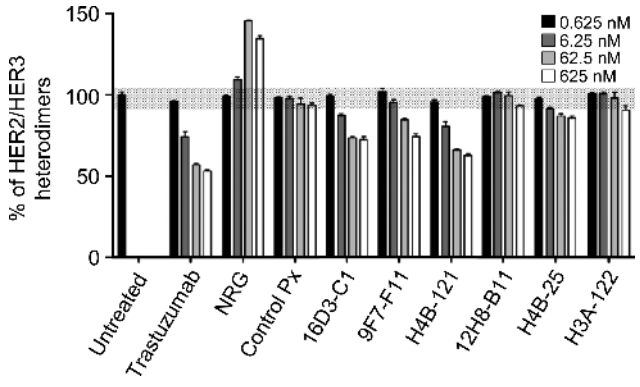


**Figure 7.** The anti–HER3 D1 Abs 16D3-C1 and 9F7-F11 and the anti-HER3 D3 Ab H4B-121, but not the Abs 12H8-B11, H4B-25, and H3A-122, block HER2/HER3 heterodimerization in NIH/3T3 fibroblasts that express HER2 and HER3. The concentration of HER3 Abs or NRG is indicated. The blockade of HER2/HER3 heterodimerization was quantified by using Ab-based TR-FRET assays.

domain, as was previously shown for cetuximab [35]. D1- and D3-specific Abs probably inhibit HER2/HER3 cellular heterodimerization by locking HER3 in a conformation that impairs the formation of HER3-containing dimers. Heterodimerization was not inhibited by the Abs H4B-25 and H3A-122 directed against the "hot-spot" D3/D4 junction, suggesting that this HER3 region is not directly involved, when D1 and D2 move further away from D3 and D4, after NRG activation, to open the receptor in an active conformation for dimerization. However, HER3 epitope targeted by D3-specific Ab H4B-25 perfectly matched with residues identified by the A30 aptamer [42], thus suggesting that this Ab could interfere with the side-by-side rearrangement of HER2/HER3 heterodimers leading to the formation of dimers, as proposed by Zhang et al. [42]. D4-specific Ab H3A-122 will rather act by sterically locked D2/D4 interdomain tether, thus hindering NRG binding [43].

An important feature of the anti–HER3 D1- and D3-specific Abs is their ability to inhibit NRG-induced phosphorylation of XIAP, FoxO1, GSK3, and MDM2. HER3 C-terminal tail has six YXXM motifs that are phosphorylated after NRG stimulation and that directly engage the N-SH2 domain of p85 and thus activate the p110 catalytic subunit

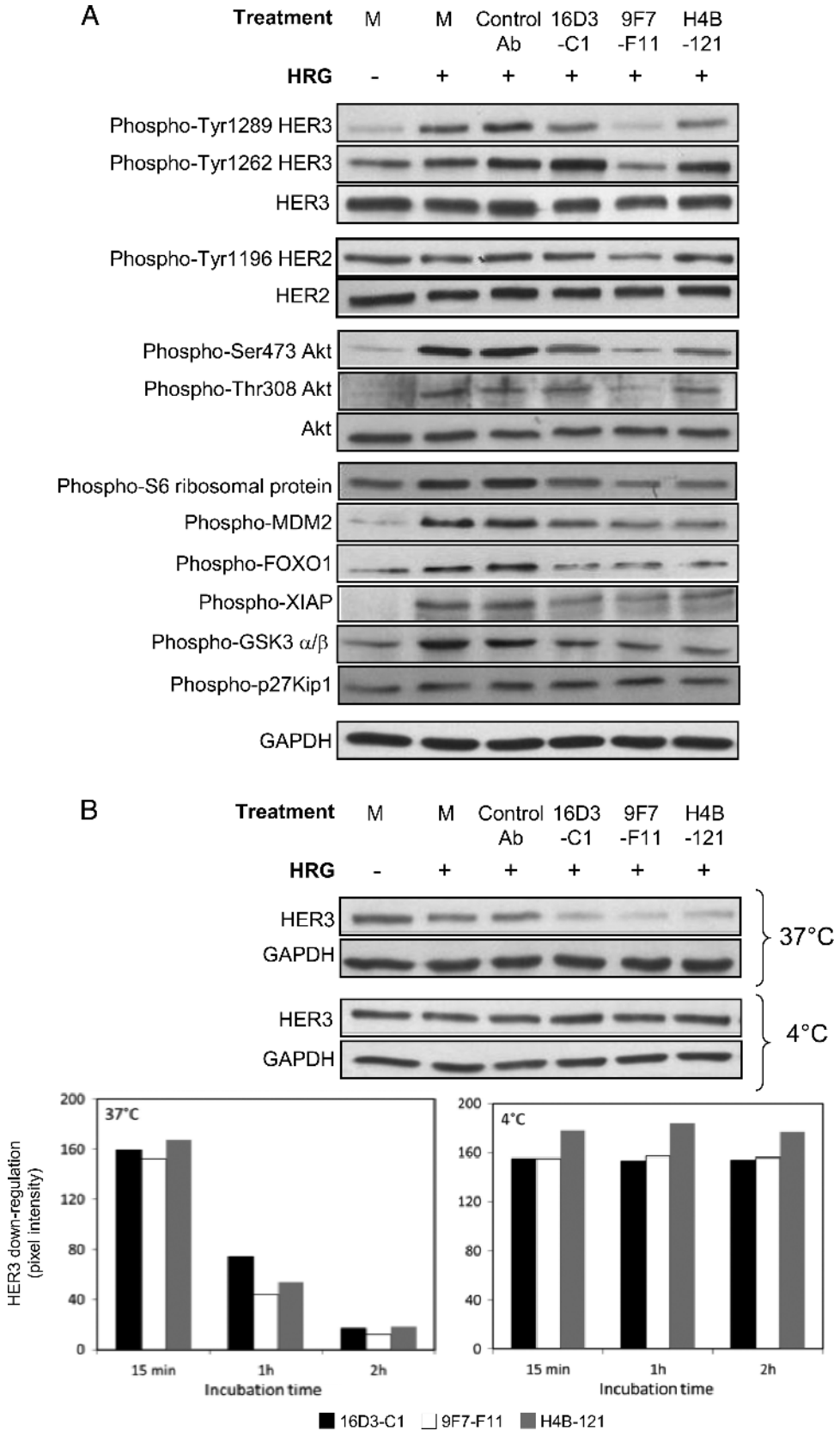


**Figure 8.** The anti–HER3 D1 Abs 16D3-C1 and 9F7-F11 and the anti-HER3 D3 Ab H4B-121 inhibit NRG-induced phosphorylation of HER3 as well as of AKT, leading to reduced phosphorylation of the downstream targets MDM2, XIAP, FoxO1, and GSK-3 (A) and to HER3 down-regulation (B). BxPC3 carcinoma cells were incubated with anti-HER3 Abs or the control Ab Px for various times and then stimulated with NRG for 10 minutes. Phosphorylation was analyzed after 15-minute Ab incubation at 37°C by Western blot analysis using the appropriate Abs. HER3 down-regulation was determined after Ab incubation at 37°C or 4°C for 15 minutes, 1 hour, and 2 hours. M, medium.

of PI3K. Recruitment and activation of PI3K leads to phosphorylation and activation of membrane-bound AKT by phosphoinositide-dependent kinase-1 (PDK1) and target of rapamycin (TOR) complex 2. Incubation with the Abs 16D3-C1 and 9F7-F11 (anti–HER3 D1) and the Ab H4B-121 (anti–HER3 D3) blocked AKT phosphorylation at $Thr^{308}$ [(induced by PDK1) and at $Ser^{473}$ (mediated by mammalian target of rapamycin (mTOR)], demonstrating that both PDK1 or mTOR signaling cascades are affected. AKT is a major signaling "hub" that phosphorylates a plethora of cell substrates and, as a consequence, can also influence tumor growth and drug resistance [5]. For instance, XIAP belongs to a family of proteins that cause innate and drug-induced resistance to apoptosis in EGFR- or HER2-positive cancer cells [44]. By inhibiting XIAP phosphorylation, our anti-HER3 Abs could favor its ubiquitination/degradation and consequently re-establish functional apoptosis in native and drug-resistant cancer cells. Nuclear FoxO1 can initiate apoptosis by inducing FasL transcription and by activating the pro-apoptotic Bcl2 family member Bim. AKT-induced phosphorylation of FoxO1 results in the export of phosphorylated FoxO1 from the nucleus to the cytoplasm and in its ubiquitination/degradation, thereby inhibiting FoxO1-dependent transcription. Overexpression of FoxO factors inhibits tumor growth *in vitro* and *in vivo* in breast cancers and FoxO cytoplasmic localization correlated with poorer survival in breast cancer patients [45]. By inhibiting FoxO1 phosphorylation, anti-HER3 Abs retain active FoxO1 in the nucleus and directly promote apoptosis of tumor cells by activating the FasL/Bcl2 pathways, as was previously demonstrated for trastuzumab [46]. However, FoxO factors also favor the transcriptional and posttranslational up-regulation of HER3 to compensate for the AKT inhibition induced by treatment with PI3K [21] and EGFR/HER2 [20,47] inhibitors in breast cancer. Therefore, dual treatment with anti-HER3 Abs (to target its drug-induced up-regulation) and kinase inhibitors should have higher anti-tumor activity. Moreover, *FoxO* knockout suppresses the induction and phosphorylation of HER3 and also of insulin receptor IGF1R [47] and the fibroblast growth factor (FGF) receptor [21], highlighting the layered interconnected tyrosine kinase receptor networks that could be concomitantly modulated by HER3-specific Abs. Finally, MDM2, an E3 ubiquitin ligase that regulates p53 by promoting its ubiquitination/degradation, also favors FoxO1 ubiquitination/degradation [48]. FoxO factors and p53 perform similar functions to enable DNA repair, maintain genomic stability, and coordinate cell cycle regulation and apoptosis through multiple tumor-suppressor mechanisms. XIAP possesses an E3 ubiquitin ligase activity that inhibits caspases 3, 7, and 9 through ubiquitination/degradation [49]. Thus anti-HER3 Abs can indirectly restore the functionality of apoptotic- and proliferative-related proteins by regulating AKT-induced ubiquitination of key components of signaling cascades, such as XIAP, MDM2/p53, and FoxO factors. In addition, p53 regulates acquired resistance and sensitivity to receptor tyrosine kinase (RTK) inhibitors [50], and anti-EGFR/HER3 Ab MEHD7945A has been recently demonstrated to increase p53 phosphorylation [41], suggesting that bypassing resistance to RTK inhibitors by modulating the p53 pathway through HER3 targeting could be an interesting way of investigation.

The binding of 9F7-F11 Ab to HER3 is NRG-independent, but this Ab inhibited ligand-induced phosphorylation of HER3 and Akt, thus confirming that it rather acts by impairing dimer formation. While a 15-minute incubation with anti-HER3 Abs was sufficient to block NRG-induced phosphorylation of HER3 and AKT, Ab-induced HER3 down-regulation in NRG-stimulated BxPC3 cells occurred later, at least after 1 hour of incubation, and persisted throughout the experiment time course. The HER3-specific Abs might thus regulate receptor quality control [4] by accelerating HER3 endocytosis, sorting, and degradation, as previously proposed by others [24–26,28]. Upon ligand binding, HER3 turnover is rapid, probably chronologically regulated by its HER heterodimerization partner (mainly HER2) and dependent on ubiquitination/deubiquitination triggered by the Nrdp1/USP8 complex [51] for degradation through the proteasomal pathway [52].

As the membrane is a "meeting point" for extracellular therapeutic Abs and intracellular pathways, we postulate that anti-HER3 Abs act by affecting HER3 membrane compartmentalization and, consequently, impairing HER heterodimerization and downstream AKT-triggered MDM2/FoxO1/XIAP signaling. Collectively, these results demonstrate that anti–HER3 D1 and D3 Abs are efficient targeted therapies to overcome drug resistance or as novel therapeutic options for pancreatic cancer and triple-negative breast cancer.

## Acknowledgments

We thank Geneviève Heintz and Sabine Bousquié for excellent technical assistance for cell culture and Ab purification, respectively. The animal facility staff is greatly acknowledged. Flow cytometry analysis was performed using equipment at the Montpellier RIO Imaging facility.

## References

[1] Yarden Y and Pines G (2012). The ERBB network: at last, cancer therapy meets systems biology. *Nat Rev Cancer* **12**, 553–563.

[2] Shi F, Telesco SE, Liu Y, Radhakrishnan R, and Lemmon MA (2010). ErbB3/HER3 intracellular domain is competent to bind ATP and catalyze autophosphorylation. *Proc Natl Acad Sci USA* **27**, 7692–7697.

[3] Ben-Kasus T, Schechter B, Lavi S, Yarden Y, and Sela M (2009). Persistent elimination of ErbB-2/HER2-overexpressing tumors using combinations of monoclonal antibodies: relevance of receptor endocytosis. *Proc Natl Acad Sci USA* **106**, 3294–3299.

[4] Carraway KL III (2010). E3 ubiquitin ligases in ErbB receptor quantity control. *Semin Cell Dev Biol* **21**, 936–943.

[5] Campbell MR, Amin D, and Moasser MM (2010). HER3 comes of age: new insights into its functions and role in signaling, tumor biology, and cancer therapy. *Clin Cancer Res* **16**, 1373–1383.

[6] Cook RS, Garrett JT, Sánchez V, Stanford JC, Young C, Chakrabarty A, Dave B, Cook RS, Pao W, McKinely E, et al. (2011). ErbB3 ablation impairs PI3K/Akt-dependent mammary tumorigenesis. *Cancer Res* **71**, 3941–3951.

[7] Friess H, Yamanaka Y, Kobrin MS, Do DA, Büchler MW, and Korc M (1995). Enhanced erbB-3 expression in human pancreatic cancer correlates with tumor progression. *Clin Cancer Res* **1**, 1413–1420.

[8] Naidu R, Yadav M, Nair S, and Kutty MK (1998). Expression of c-erbB3 protein in primary breast carcinomas. *Br J Cancer* **78**, 1385–1390.

[9] Tanner B, Hasenclever D, Stern K, Schormann W, Bezler M, Hermes M, Brulport M, Bauer A, Schiffer IB, Gebhard S, et al. (2006). ErbB-3 predicts survival in ovarian cancer. *J Clin Oncol* **24**, 4317–4323.

[10] Reschke M, Mihic-Probst D, van der Horst EH, Knyazev P, Wild PJ, Hutterer M, Meyer S, Dummer R, Moch H, and Ullrich A (2008). HER3 is a determinant for poor prognosis in melanoma. *Clin Cancer Res* **14**, 5188–5197.

[11] Hayashi M, Inokuchi M, Takagi Y, Yamada H, Kojima K, Kumagai J, Kawano T, and Sugihara K (2008). High expression of HER3 is associated with a decreased survival in gastric cancer. *Clin Cancer Res* **14**, 7843–7849.

[12] Takikita M, Xie R, Chung JY, Cho H, Ylaya K, Hong SM, Moskaluk CA, and Hewitt SM (2011). Membranous expression of HER3 is associated with a decreased survival in head and neck squamous cell carcinoma. *J Transl Med* **9**, 126–136.

[13] Beji A, Horst D, Engel J, Kirchner T, and Ullrich A (2012). Toward the prognostic significance and therapeutic potential of HER3 receptor tyrosine kinase in human colon cancer. *Clin Cancer Res* **18**, 956–968.

[14] Ho-Pun-Cheung A, Assenat E, Bascoul-Mollevi C, Bibeau F, Boissière-Michot F, Cellier D, Azria D, Rouanet P, Senesse P, Ychou M, et al. (2011). EGFR and HER3 mRNA expression levels predict distant metastases in locally advanced rectal cancer. *Int J Cancer* **128**, 2938–2946.

[15] Narayan M, Wilken JA, Harris LN, Baron AT, Kimbler KD, and Maihle NJ (2009). Trastuzumab-induced HER reprogramming in "resistant" breast carcinoma cells. *Cancer Res* **69**, 2191–2194.

[16] Wheeler DL, Huang S, Kruser TJ, Nechrebecki MM, Armstrong EA, Benavente S, Gondi V, Hsu KT, and Harari PM (2008). Mechanisms of acquired resistance to cetuximab: role of HER (ErbB) family members. *Oncogene* **27**, 3944–3956.

[17] Yonesaka K, Zejnullahu K, Okamoto I, Satoh T, Cappuzzo F, Souglakos J, Ercan D, Rogers A, Roncalli M, Takeda M, et al. (2011). Activation of ERBB2 signaling causes resistance to the EGFR-directed therapeutic antibody cetuximab. *Sci Transl Med* **3**, 99ra86.

[18] Arnoletti JP, Buchsbaum DJ, Huang ZQ, Hawkins AE, Khazaeli MB, Kraus MH, and Vickers SM (2004). Mechanisms of resistance to Erbitux (anti-epidermal growth factor receptor) combination therapy in pancreatic adenocarcinoma cells. *J Gastrointest Surg* **8**, 960–969.

[19] Engelman JA, Zejnullahu K, Mitsudomi T, Song Y, Hyland C, Park JO, Lindeman N, Gale CM, Zhao X, Christensen J, et al. (2007). MET amplification leads to gefitinib resistance in lung cancer by activating ERBB3 signaling. *Science* **316**, 1039–1043.

[20] Garrett JT, Olivares MG, Rinehart C, Granja-Ingram ND, Sánchez V, Chakrabarty A, Dave B, Cook RS, Pao W, McKinely E, et al. (2011). Transcriptional and posttranslational up-regulation of HER3 (ErbB3) compensates for inhibition of the HER2 tyrosine kinase. *Proc Natl Acad Sci USA* **108**, 5021–5026.

[21] Chakrabarty A, Sánchez V, Kuba MG, Rinehart C, and Arteaga CL (2011). Feedback upregulation of HER3 (ErbB3) expression and activity attenuates antitumor effect of PI3K inhibitors. *Proc Natl Acad Sci USA* **109**, 2718–2723.

[22] Desbois-Mouthon C, Baron A, Blivet-Van Eggelpoël MJ, Fartoux L, Venot C, Bladt F, Housset C, and Rosmorduc O (2009). Insulin-like growth factor-1 receptor inhibition induces a resistance mechanism via the epidermal growth factor receptor/HER3/AKT signaling pathway: rational basis for cotargeting insulin-like growth factor-1 receptor and epidermal growth factor receptor in hepatocellular carcinoma. *Clin Cancer Res* **15**, 5445–5456.

[23] Kruser TJ and Wheeler DL (2010). Mechanisms of resistance to HER family targeting antibodies. *Exp Cell Res* **316**, 1083–1100.

[24] van der Horst EH, Murgia M, Treder M, and Ullrich A (2005). Anti-HER-3 MAbs inhibit HER-3-mediated signaling in breast cancer cell lines resistant to anti-HER-2 antibodies. *Int J Cancer* **115**, 519–527.

[25] Schoeberl B, Faber AC, Li D, Liang MC, Crosby K, Onsum M, Burenkova O, Pace E, Walton Z, Nie L, et al. (2010). An ErbB3 antibody, MM-121, is active in cancers with ligand-dependent activation. *Cancer Res* **70**, 2485–2494.

[26] Sala G, Traini S, D'Egidio M, Vianale G, Rossi C, Piccolo E, Lattanzio R, Piantelli M, Tinari N, Natali PG, et al. (2012). An ErbB-3 antibody, MP-RM-1, inhibits tumor growth by blocking ligand-dependent and independent activation of ErbB-3/Akt signaling. *Oncogene* **31**, 1275–1286.

[27] Schaefer G, Haber L, Crocker LM, Shia S, Shao L, Dowbenko D, Totpal K, Wong A, Lee CV, Stawicki S, et al. (2011). A two-in-one antibody against HER3 and EGFR has superior inhibitory activity compared with monospecific antibodies. *Cancer Cell* **20**, 472–486.

[28] Aurisicchio L, Marra E, Luberto L, Carlomosti F, De Vitis C, Noto A, Gunes Z, Roscilli G, Mesiti G, Mancini R, et al. (2012). Novel anti-ErbB3 monoclonal antibodies show therapeutic efficacy in xenografted and spontaneous mouse tumors. *J Cell Physiol* **227**, 3381–3388.

[29] Blackburn E, Zona S, Murphy ML, Brown IR, Chan SK, and Gullick WJ (2012). A monoclonal antibody to the human HER3 receptor inhibits Neuregulin 1-beta binding and co-operates with Herceptin in inhibiting the growth of breast cancer derived cell lines. *Breast Cancer Res Treat* **134**, 53–59.

[30] Sheng Q, Liu X, Fleming E, Yuan K, Piao H, Chen J, Moustafa Z, Thomas RK, Greulich H, Schinzel A, et al. (2010). An activated ErbB3/NRG1 autocrine loop supports *in vivo* proliferation in ovarian cancer cells. *Cancer Cell* **17**, 298–310.

[31] Schmiedel J, Blaukat A, Li S, Knöchel T, and Ferguson KM (2008). Matuzumab binding to EGFR prevents the conformational rearrangement required for dimerization. *Cancer Cell* **13**, 365–373.

[32] Gaborit N, Larbouret C, Vallaghe J, Peyrusson F, Bascoul-Mollevi C, Crapez E, Azria D, Chardès T, Poul MA, Mathis G, et al. (2011). Time-resolved fluorescence resonance energy transfer (TR-FRET) to analyze the disruption of EGFR/HER2 dimers: a new method to evaluate the efficiency of targeted therapy using monoclonal antibodies. *J Biol Chem* **286**, 11337–11345.

[33] Mondon P, Souyris N, Douchy L, Crozet F, Bouayadi K, and Kharrat H (2007). Method for generation of human hyperdiversified antibody fragment library. *Biotechnol J* **2**, 76–82.

[34] Talavera A, Friemann R, Gómez-Puerta S, Martinez-Fleites C, Garrido G, Rabasa A, López-Requena A, Pupo A, Johansen RF, Sénchez O, et al. (2009). Nimotuzumab, an antitumor antibody that targets the epidermal growth factor receptor, blocks ligand binding while permitting the active receptor conformation. *Cancer Res* **69**, 5851–5859.

[35] Li S, Schmitz KR, Jeffrey PD, Wiltzius JJ, Kussie P, and Ferguson KM (2005). Structural basis for inhibition of the epidermal growth factor receptor by cetuximab. *Cancer Cell* **7**, 301–311.

[36] Larbouret C, Robert B, Navarro-Teulon I, Thèzenas S, Ladjemi MZ, Morisseau S, Campigna E, Bibeau F, Mach JP, Pèlegrin A, et al. (2007). *In vivo* therapeutic synergism of anti-epidermal growth factor receptor and anti-HER2 monoclonal antibodies against pancreatic carcinomas. *Clin Cancer Res* **13**, 3356–3362.

[37] Zhou BB, Peyton M, He B, Liu C, Girard L, Caudler E, Lo Y, Baribaud F, Mikami I, Reguart N, et al. (2006). Targeting ADAM-mediated ligand cleavage to inhibit HER3 and EGFR pathways in non-small cell lung cancer. *Cancer Cell* **10**, 39–50.

[38] Farhan H, Schuster C, Klinger M, Weisz E, Waxenecke G, Schuster M, Sexl V, Mudde GC, Freissmuth M, and Kircheis R (2006). Inhibition of xenograft tumor growth and down-regulation of ErbB receptors by an antibody directed against Lewis Y antigen. *J Pharmacol Exp Ther* **319**, 1459–1466.

[39] Nakamura H, Takamori S, Fujii T, Ono M, Yamana H, Kuwano M, and Shirouzu K (2005). Cooperative cell-growth inhibition by combination treatment with ZD1839 (Iressa) and trastuzumab (Herceptin) in non-small-cell lung cancer. *Cancer Lett* **230**, 33–46.

[40] McDonagh CF, Huhalov A, Harms BD, Adams S, Paragas V, Oyama S, Zhang B, Luus L, Overland R, Nguyen S, et al. (2012). Antitumor activity of a novel bispecific antibody that targets the ErbB2/ErbB3 oncogenic unit and inhibits heregulin-induced activation of ErbB3. *Mol Cancer Ther* **11**, 582–593.

[41] Huang SM, Li C, Armstrong EA, Peet CR, Saker J, Amler LC, Sliwkowski MX, and Harari P (2012). Dual targeting of EGFR and HER3 with MEHD7945A overcomes acquired resistance to EGFR inhibitors and radiation. *Cancer Res* **73**, 824–833.

[42] Zhang Q, Park E, Kani K, and Landgraf R (2012). Functional isolation of activated and unilaterally phosphorylated heterodimers of ERBB2 and ERBB3 as scaffolds in ligand-dependent signaling. *Proc Natl Acad Sci USA* **109**, 13237–13242.

[43] Cho HS and Leahy DJ (2002). Structure of the extracellular region of HER3 reveals an interdomain tether. *Science* **297**, 1330–1333.

[44] Aird KM, Ding X, Baras A, Wei J, Morse MA, Clay T, Lyerly HK, and Devi GR (2008). Trastuzumab signaling in ErbB2-overexpressing inflammatory breast cancer correlates with X-linked inhibitor of apoptosis protein expression. *Mol Cancer Ther* **7**, 38–47.

[45] Yang JY, Zong CS, Xia W, Yamaguchi H, Ding Q, Xie X, Lang JY, Lai CC, Chang CJ, Huang WC, et al. (2008). ERK promotes tumorigenesis by inhibiting FOXO3a via MDM2-mediated degradation. *Nat Cell Biol* **10**, 138–148.

[46] Wu Y, Shang X, Sarkissyan M, Slamon D, and Vadgama JV (2010). FOXO1A is a target for HER2-overexpressing breast tumors. *Cancer Res* **70**, 5475–5485.

[47] Chandarlapaty S, Sawai A, Scaltriti M, Rodrik-Outmezgui V, Grbovic-Huezo O, Serra V, Majumder PK, Baselga J, and Rosen N (2011). AKT inhibition relieves feedback suppression of receptor tyrosine kinase expression and activity. *Cancer Cell* **19**, 58–71.

[48] Fu W, Ma Q, Chen L, Li P, Zhang M, Ramamoorthy S, Nawaz Z, Shimojima T, Wang H, Yang Y, et al. (2009). MDM2 acts downstream of p53 as an E3 ligase to promote FOXO ubiquitination and degradation. *J Biol Chem* **284**, 13987–14000.

[49] Eckelman BP, Salvesen GS, and Scott FL (2006). Human inhibitor of apoptosis proteins: why XIAP is the black sheep of the family. *EMBO Rep* **7**, 988–994.

[50] Huang S, Benavente S, Armstrong EA, Li C, Wheeler DL, and Harari PM (2011). p53 modulates acquired resistance to EGFR inhibitors and radiation. *Cancer Res* **71**, 7071–7079.

[51] Cao Z, Wu X, Yen L, Sweeney C, and Carraway KL III (2007). Neuregulin-induced ErbB3 downregulation is mediated by a protein stability cascade involving the E3 ubiquitin ligase Nrdp1. *Mol Cell Biol* **27**, 2180–2188.

[52] Qiu XB and Goldberg AL (2002). Nrdp1/FLRF is a ubiquitin ligase promoting ubiquitination and degradation of the epidermal growth factor receptor family member, ErbB3. *Proc Natl Acad Sci USA* **99**, 14843–14848.

## Supplementary Materials

### *Cell Lines*

The human pancreatic (BxPC-3), breast (MDA-MB-468), epidermoid (A431), and lung (A549) cancer cell lines were from ATCC. The mouse embryonic fibroblast NIH/3T3 cell line was kindly provided by S. Schmidt (CNRS-UMR 5237, Montpellier, France). EGFR-, HER2-, HER3-, HER2/HER3-, and EGFR/HER4-transfected NIH/3T3 cell lines were obtained as previously described [32]. BxPC-3 cells were cultured in RPMI 1640; NIH/3T3, A431, A549, and MDA-MB-468 cells were cultured in Dulbecco's modified Eagle's medium. The complete culture media were supplemented as recommended by ATCC, usually with 10% FCS. All culture media and supplements were purchased from Life Technologies, Inc (Gibco BRL, Gaithersburg, MD). Cells were grown at 37°C in a humidified atmosphere of 5% $CO_2$ and medium was replaced twice a week.

### *Ab Generation*

As previously described [33], the human scFv phage library (MG-Umab) was generated by combining donor Ab sequences obtained from a wide naive Ab population and a naturally oriented Ab population against several pathologies (100 donors). It was then further customized by random mutagenesis of the entire variable domain, thus mimicking the *in vivo* process of Ab diversity, and finally cloned in fusion with the *β-lactamase* gene to eliminate premature stop codon sequences. To select HER3-binding clones, the library MG-Umab (size, $3.4 \times 10^9$; 94% of clones coding full-length Abs) was subjected to four rounds of selection in eight-well MaxiSorp immunoplates that had been previously coated with 1 μg of HER3-Fc. For the last three rounds of selection, a depletion step with human $IgG_1$ was introduced before incubation to avoid the selection of Fc binders. After selection, 96 individual phage-infected colonies from the third round and 48 from the fourth round of selection were randomly picked and used to produce phage-scFv particles in 96-well plates. HER3-specific phage-scFv were screened by ELISA using 500 ng/ml HER3-Fc as target and HRP-labeled anti-M13 secondary Ab (1/10,000 dilution; GE Healthcare, Chalfont, United Kingdom) as detection Ab. Each phage-scFv was tested simultaneously for binding to HER3-Fc and to BSA (control) as control. Nine clones showing the higher positive signal (HER3 signal up to three times stronger than the BSA signal) were sequenced and expressed as fully human $IgG_1$ for further characterization.

To obtain HER3-specific mouse monoclonal Abs, BALB/c mice were injected subcutaneously with 10 μg of soluble HER3-Fc or intraperitoneally with $2 \times 10^6$ HER2/HER3-transfected NIH/3T3 cells (previously stimulated with 100 ng/ml NRG to favor HER2/HER3 heterodimer formation) at days 0, 14, and 28. To monitor the Ab response, Ab titers were measured by ELISA or flow cytometry. After a last boost with the antigens 3 days before fusion, spleen cells from one HER3-Fc–immunized and one HER2/HER3 NIH/3T3-immunized mouse were fused according to the protocol already described using the PX63Ag8.653 myeloma cell line. Fused cells were cultured in 96-well plates (100,000 cells/well) with hypoxanthine-aminopterin-thymidine (HAT) medium for hybridoma selection. Hybridoma supernatant screening was performed by ELISA using 250 ng/ml HER3-Fc or Fc alone (control) as antigens at day 12 post-fusion. Ten HER3-specific hybridomas were cryopreserved and cloned before experiments. The hybridoma cell line that produces the anti-HER3 Ab 16D3-C1 was deposited in the Collection Nationale de Cultures de Microorganismes (Institut Pasteur, Paris, France) under the reference CNCM I-4486.

### *HER3 Binding Studies*

The binding specificity of selected Abs to soluble HER3 was assessed by ELISA. ELISA 96-well microplates (Nunc, Paisley, United Kingdom) were coated with 250 ng/ml human or mouse HER3-Fc antigen in PBS buffer at 4°C overnight. After four washes in PBS/0.1% Tween 20 (PBS-T) and saturation with 1% BSA in PBS-T at 37°C for 1 hour, 100 μl of 1 μg/ml dilution of anti-HER3 Abs in PBS-T were added to each well. After incubation for 2 hours and four washes in PBS-T, bound Abs were detected by incubation with peroxidase-conjugated goat $F(ab)'_2$ polyclonal Abs (1:10,000 dilution) against human or mouse $F(ab)'_2$ fragments (Jackson ImmunoResearch) for 1 hour, followed by addition of the peroxidase substrate. Absorbance was measured at 450 nm. Three replicates of each dilution were performed and each experiment was done three times; shown data correspond to the mean value of absorbance ± SD.

The kinetic parameters of the binding of selected Abs to HER3 were determined at 25°C by surface plasmon resonance analysis using a BIACORE 3000 instrument (BIACORE AB, Uppsala, Sweden). HER3-specific Abs were immobilized on the CM5 sensor chip surface using a rabbit anti-mouse or anti-human polyclonal Ab (Sigma-Aldrich) according to the manufacturer's instructions. Recombinant HER3 in HBS-EP buffer [10 mM Hepes (pH 7.4), 3 mM EDTA, 150 mM NaCl, and 0.005% non-ionic surfactant P20 (GE Healthcare)] was injected at concentrations between 3.12 and 200 nM over the flow cell, and the dissociation phase was followed by a regeneration step with 10 mM HCl solution. The flow rate was 50 μl/min. All sensorgrams were corrected by subtracting the control flow cell signal. Data were globally fitted to a Langmuir 1:1 model using the BIAevaluation version 4.1.1 software.

The binding specificity of selected Abs to membrane HER3 was assessed by flow cytometry. One million HER3- and HER2/HER3-transfected NIH/3T3 cells or control cells (parental NIH/3T3 cells, EGFR-, HER2-, and EGFR/HER4-transfected cells) [32] were incubated with 20 μg/ml anti-HER3 Abs in PBS buffer without $Ca^{++}$ and $Mg^{++}$ and supplemented with 1% BSA (PBS–1% BSA) at 4°C for 1.5 hours. After three washes in PBS–1% BSA, cells were incubated with fluorescein-conjugated goat anti-human (1:60) or anti-mouse (1:100) Fc Abs (Sigma-Aldrich) in the dark at 4°C for 1 hour. Cells were then washed three times and suspended in PBS for analysis using an FC500 flow cytometer (Beckman Coulter).

### *Western Blot Analysis*

BxPC3 tumor cells were plated at 500,000 cells/well in six-well culture plates and cultured at 37°C for 24 hours. After serum starvation in RPMI complete medium with 1% FCS for 16 hours, cells were washed and pre-incubated in 50 μg/ml anti-HER3 Abs or Px Ab (negative control) at different temperatures and for various times, before washing and stimulation with 100 ng/ml NRG for 10 minutes. Cells were then washed, scraped, and lysed with buffer containing 20 mM Tris-HCl (pH 7.5), 150 mM NaCl, 1.5 mM $MgCl_2$, 1 mM EDTA, 1% Triton, 10% glycerol, 0.1 mM phenylmethylsulfonyl fluoride, 100 mM sodium fluoride, 1 mM sodium orthovanadate (Sigma-Aldrich), and one tablet of complete protease inhibitor mixture (Roche Diagnostics, Indianapolis, IN). After 30 minutes, the insoluble fraction was eliminated by centrifugation and protein concentrations in

cell lysates were determined by the Bradford assay. Protein lysates were directly mixed with Laemmli buffer and heated at 95°C for 5 minutes. After sodium dodecyl sulfate–polyacrylamide gel electrophoresis under reducing conditions, proteins were transferred to polyvinylidene difluoride membranes (Millipore), which were then saturated in TNT buffer [25 mM Tris (pH 7.4), 150 mM NaCl, 0.1% Tween] containing 5% non-fat dry milk at 25°C for 1 hour. Membranes were incubated with primary Abs against kinase receptors or signaling kinases and their phosphorylated forms in TNT/5% BSA buffer at 4°C for 18 hours. After five washes in TNT buffer, peroxidase-conjugated rabbit, goat, or mouse polyclonal Abs (Sigma-Aldrich) were added, as appropriate, in TNT buffer containing 5% non-fat dry milk at 25°C for 1 hour. After five washes in TNT buffer, blots were visualized using a chemiluminescent substrate (Western Lightning Plus-ECL; PerkinElmer).

### *HTRF Analysis of HER2/HER3 Heterodimerization*

HER2/HER3 heterodimers were quantified using Ab-based TR-FRET assay, as previously described [32]. The assay was performed on adherent cells using the anti-HER2 Ab FRP5 and the anti-HER3 Ab 15D4-F2 that were labeled with Lumi4-terbium cryptate or D2 acceptor dye, respectively (Cisbio Bioassays, Bagnol-sur-Cèze, France). These Abs recognize epitopes that are different from those of the Abs under study, and thus, no interference was observed in the TR-FRET assay (data not shown). HER2/HER3-transfected NIH/3T3 cells were plated at $3 \times 10^5$ per well in 96-well sterile black microplates in Dulbecco's modified Eagle's medium (without phenol red) supplemented with 10% FCS. After 24 hours, cells were incubated with the anti-HER3 Abs or NRG at concentrations ranging from 0.625 nM to 625 nM at 37°C for 30 minutes. After washing in KREBS buffer, cells were fixed in 10% formalin (Sigma-Aldrich) for 2 minutes and washed once with KREBS. After incubation with 5 nM FRP5 and 15D4-F2 in KREBS buffer at 37°C for 6 hours, cells were washed four times with KREBS buffer. The fluorescence of Lumi4-terbium and D2 were measured, respectively, at 620 and 665 nm (60-μs delay and 400-μs integration) upon 337-nm excitation on a Pherastar FS instrument (BMG Labtech, Offenburg, Germany). The TR-FRET signal was expressed as $\Delta F665(\%) = \Delta F665/F665_{Tb}$, with $\Delta F665 = F665c - F665_{Tb}$, as previously explained [32], and then data were presented considering the untreated sample as having 100% dimerization.